Yao et al. Nanoscale Research Letters (2016) 11:511
DOI 10.1186/s11671-016-1736-7

Nanoscale Research Letters

NANO EXPRESS Open Access

The Luminescent Inhomogeneity and the Distribution of Zinc Vacancy-Related Acceptor-Like Defects in N-Doped ZnO Microrods

Zhengrong Yao[1,2], Kun Tang[1*], Zhonghua Xu[1], Jiandong Ye[1], Shunming Zhu[1] and Shulin Gu[1*]

Abstract

Vertically aligned N-doped ZnO microrods with a hexagonal symmetry were fabricated via the chemical vapor transport with abundant N_2O as both O and N precursors. We have demonstrated the suppression of the zinc interstitial-related shallow donor defects and have identified the zinc vacancy-related shallow and deep acceptor states by temperature variable photoluminescence in O-rich growth environment. Through spatially resolved cathodoluminescence spectra, we found the luminescent inhomogeneity in the sample with a core-shell structure. The deep acceptor-isolated V_{Zn} and the shallow acceptor V_{Zn}-related complex or clusters mainly distribute in the shell region.

Keywords: Zinc oxide, Microrod, Chemical vapor transport, Defect identification and distribution, Spatially resolved cathodoluminescence

Background

It is well-known that efficient p-type doping in ZnO thin films is extremely hard partially due to the very limited dopant solubility in high-quality lattice [1, 2]. Dopants are found to distribute along grain boundaries possibly due to the relatively degraded crystalline quality there. Grain boundaries would form low-resistive electrical channels, and the carrier transport is thus dominated by them, which has no practical significance [3]. However, micro-/nanostructured ZnO materials may provide an alternative to realize considerable doping efficiency by utilizing abundant surface areas. Similar as grain boundaries in thin films, surface areas in micro-/nanostructured ZnO are more chemically active, which results in lowered formation energies for impurities or defects. Therefore, doping is thought to be much easier on surfaces.

However, owing to such a different impurity or defect incorporation ability between bulk and surface, a spatially inhomogeneous distribution of the impurities or defects will naturally occur in ZnO micro-/nanostructures. Several groups have reported the inhomogeneity in terms of luminescent characterizations. Shalish et al. [4] have found that the luminescent intensity ratio between the below bandgap (surface) and the near band edge (NBE) emissions in ZnO nanowires depends on the wire radius. Pan et al. [5] have observed an increased intensity of deep-level (DL) emission when the surface aspect ratio becomes higher in their tapered ZnO nanorod. Foley et al. [6] have observed that the cathodoluminescence (CL) characteristics vary dramatically between the tip and sidewall of the ZnO nanorod as well as CL excitation depth. They also suggested that the green band (GB) luminescence originating from the ZnO surface is likely caused by oxygen vacancy (V_O). Khranovskyy et al. [7] have further revealed that the NBE emission occurs primarily from the top (0001) planes of ZnO microrods (MRs) while the point defect V_O-related visible emission mainly occurs from the side facets. Liao and Zhang [8] and Kaftelen et al. [9] have both reported that the ZnO nanostructures have a core-shell-structured luminescent distribution, and the visible luminescence is mainly emitted from the surface region where large numbers of V_O exist. However, Fabbri et al.

* Correspondence: ktang@nju.edu.cn; slgu@nju.edu.cn
[1]School of Electronic Science and Engineering, Nanjing University, Nanjing 210023, China
Full list of author information is available at the end of the article

[10] unambiguously gave the first evidence that zinc vacancy (V_{Zn}) at the (10-10) non-polar surfaces is responsible for the GB luminescence of ZnO nanostructures by performing an exhaustive comparison between CL spectra and imaging and ab initio simulations.

All these prior literatures have demonstrated the luminescent inhomogeneity in ZnO micro-/nanostructures and that spatially resolved (SR) CL is a powerful tool to investigate this issue. However, the correlation between the DL (or GB) and the NBE luminescence and the responsible defects have not yet been fully established, leading to highly controversial attributions. Furthermore, none of the previous works has given information on the distribution of shallow acceptors in ZnO micro-/nanostructures, which is of crucial importance for further design and optimization of ZnO-based nanostructure devices. As a result, in order to explore the correlation between the luminescence and defects and the distribution of defects in the nanostructured ZnO material, we have employed Raman spectra, electrical characterization, low-temperature SR-CL, and temperature-dependent (TD) photoluminescence (PL) on our N-doped ZnO MR array samples. The experimental results have demonstrated the inhomogeneous luminescent distribution, and it was found out that the native defect-isolated V_{Zn} [11, 12] connected with the GB emissions and the shallow acceptors originating from V_{Zn}-related complexes [13, 14] or clusters [15, 16] are mainly located at the shell region of the MRs.

Methods

Vertically aligned N-doped ZnO MR array samples were homo-epitaxially grown on a high-quality ZnO template via chemical vapor transport method without any catalyst. The carrier gas was 100 SCCM N_2, and 8 SCCM N_2O was employed as both O and N precursors. A radio frequency plasma generator was used to ionize N_2O to produce efficient O and N atoms. The detail of procedure and conditions can be referenced elsewhere [12].

The morphologies of the as-grown samples were characterized by JEOL JSM-7000F scanning electron microscopy (SEM), attached with a Gatan MonoCL system. The chemical configuration of the elements was determined by X-ray photoelectron spectrometry (XPS) with an Al Kα X-ray monochromatic source at 1486.6 eV. Ar ion etching was performed in order to avoid the influence of surface absorption in the atmosphere, and the binding energy was calibrated by the C 1s peak at 285 eV. High-resolution X-ray diffraction (XRD) spectra were recorded to study the crystallinity of the samples on a Philips X'pert Pro diffractometer. The vibrational properties of the samples were investigated by a JOBIN YVON HR800 Raman system in the backscattering geometry with 514-nm radiation at room temperature. For analyzing the luminescence properties of a single MR, TD-PL excited by a He–Cd laser at the wavelength of 325 nm and SR-CL using variable acceleration voltage from 3 to 15 kV were carried out. The CL spectra and monochromatic imaging in this work were performed at the temperature of 100 K. To get the electrical parameters of N-doped ZnO MRs, back-gate field effect transistors (FETs) of a single MR were fabricated and measured.

Results and Discussion

Figure 1 shows the morphologies of the as-grown N-doped ZnO MR array. The images from top view and side view show an array of vertically well-aligned MRs with a hexagonal symmetry, which are parallel to each other. The in-plane scale of most MRs is around 1 μm while the height is around several microns. It is clear that there is a "foam-like" network of nanowalls below the MRs, which is entirely consistent with the experimental results reported previously [17, 18]. Since the metal catalyst was not used, the growth mechanism of the ZnO MRs is different from the traditional vapor–liquid–solid (VLS) mechanism and apparently via vapor–solid mechanism or the self-catalyzed VLS mechanism as proposed by Hu et al. [19]. When the growth process was over, the furnace was cooled down naturally to room temperature. However, the carbothermal reduction reaction did not stop immediately at the beginning of the cooling process due to the high furnace temperature. Therefore, the reaction of small amount of residual Zn and O atoms would form a layer of hexagonal head on the top of some MRs, as observed in Fig. 1.

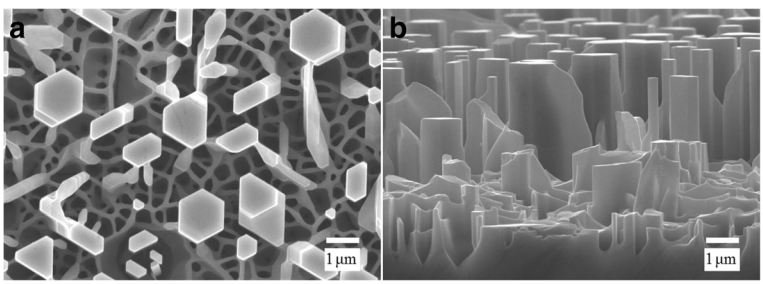

Fig. 1 The **a** top view and **b** side-view SEM images of the vertically aligned N-doped ZnO MRs

In order to investigate the chemical configuration of the elements in N-doped ZnO MRs, XPS was performed on the MR sample after Ar ion etching. As shown in Fig. 2a, we have observed two N 1s signals located around 396 and 401 eV, respectively, confirming the incorporation of N in our sample. Literatures show that the binding energy of the N 1s signal is very sensitive to the chemical environment. It has been reported that N can be incorporated into ZnO lattice in at least two chemical states, either as a N atom or a N_2 molecule occupying an O site (N_O or $(N_2)_O$), corresponding to the peaks at 396.5 and 404.5 eV, respectively [20]. Wei et al. [21] have observed three features in the N 1s XPS spectra located at 396, 400, and 402 eV and have identified them as the N–Zn bond related to atomic N (β-N), well-screened and poorly screened molecular N (γ-N_2), respectively. Therefore, we assigned the N 1s signals of 396 and 401 eV to β-N and γ-N_2, respectively, indicating the formation of N_O and $(N_2)_O$ defects in our N-doped ZnO MRs.

The typical asymmetric O 1s peak of N-doped ZnO MRs is shown in Fig. 2b, which can be consistently fitted by three nearly Gaussian components, centered at 530.3, 531.9, and 532.6 eV, respectively. The main component on the low binding energy side can be attributed to the O–Zn bond, while the component with high binding energy is usually attributed to chemisorbed or dissociated OH or O species on the surface of ZnO material [22]. Then, according to the literature [23], the middle component is associated with O^{2-} ions in the O deficient regions within the ZnO lattice, and the intensity of this component may be partially connected with the concentration of V_O, which has the lowest formation energy among the donor-like defects [24]. In addition, the XPS O 1s peak of undoped ZnO MRs grown with 1 SCCM high-purity O_2 [12] is shown in Fig. 2c for comparison. It is obvious that the intensity of V_O-related component in undoped sample is stronger than that of N-doped sample grown with higher VI/II ratio, indicating that V_O could be suppressed in O-rich growth environment to a great extent.

The XRD and Raman characterizations have also demonstrated high crystalline quality for the sample. As seen from Fig. 3, only the ZnO (0002) in addition to the Al_2O_3 (0006) diffraction peaks can be observed, indicating that the ZnO MRs are oriented along the *c* axis with a well-ordered wurtzite structure. The full width at half maximum (FWHM) of the rocking curve (XRC) for the ZnO (0002) peak is 0.1252° as shown in the inset of Fig. 3, suggesting an excellent crystalline quality of the N-doped ZnO MRs. Raman spectrum (also shown in the inset of Fig. 3) shows classical ZnO lattice-related modes E_2(low), $2E_2$(M), E_2(high), and A_1(longitudinal optical (LO)), located at 99, 332, 438, and 579 cm^{-1}, respectively. The narrow width and high intensity of E_2(low) and E_2(high) are also an indication of high material quality. Moreover, in a previous paper, we observed additional modes (AMs) at 276, 510, 582, and 644 cm^{-1} in the Raman spectrum of N-doped ZnO MRs grown by 1 SCCM of N_2O, while these AMs were absent in undoped ZnO MRs grown with high-purity O_2 as O source [12]. It has been reported that the formation

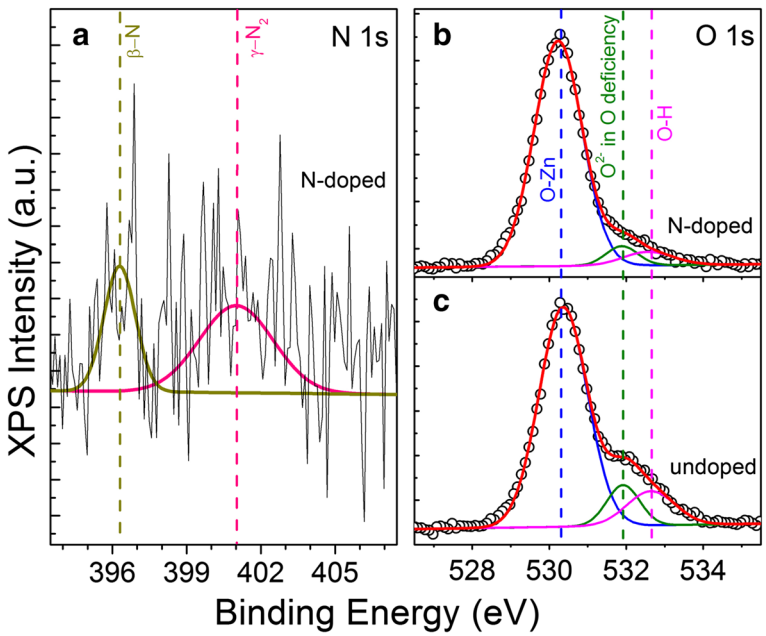

Fig. 2 **a** The XPS N 1s spectrum of N-doped ZnO MRs. The XPS O 1s peaks of **b** N-doped and **c** undoped ZnO MRs

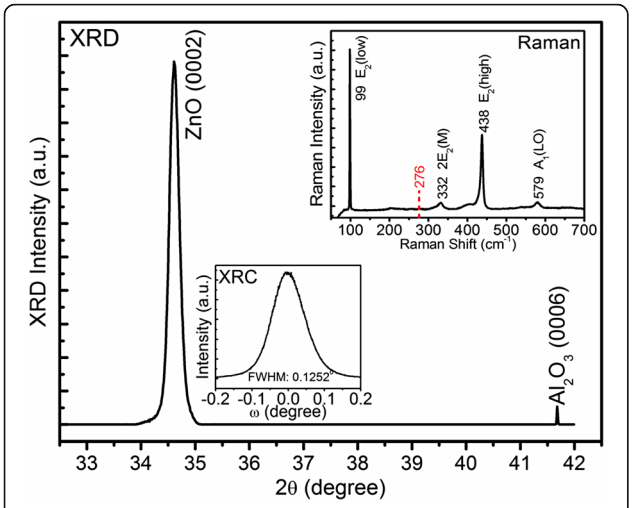

Fig. 3 The XRD ω-2θ pattern of the N-doped ZnO MRs. The two *insets* depict the XRC of ZnO (0002) peak and the Raman spectra recorded at room temperature, respectively

energy of native defect zinc interstitial (Zn_i) increases in O-rich growth environment via a comprehensive first-principle investigation based on density functional theory [24]. Besides, Gluba et al. [25] reported that the AM at 274 cm^{-1} is related to small Zn_i clusters, which can be suppressed when the ZnO sample is deposited under O_2 plasma. Lately, combined with defect formation energy calculations, Zhang et al. [26] demonstrated that Zn_i can be increased by the incorporation of N_O but suppressed by the presence of $(N_2)_O$. Consequently, considering higher O partial pressure in gas phase due to higher flow rate of N_2O and the $(N_2)_O$ signal at 401 eV in the N 1s XPS spectrum, that no such AMs can be detected in the inset of Fig. 3 indicates a suppression of Zn_i small cluster-related native donors.

In ref. [12], we have discussed the optical properties of the undoped ZnO MRs in detail, and the NBE emission recorded at 9 K is dominated by excitons bound to neutral donors (D^0X) and its two phonon replicas, located at 3.362, 3.291, and 3.218 eV, respectively. Provided the incorporation of N and the suppression of such a chief native donor Zn_i, as shown in Fig. 4, the strongest NBE emission peak at 3.359 eV in the 9 K PL spectrum of

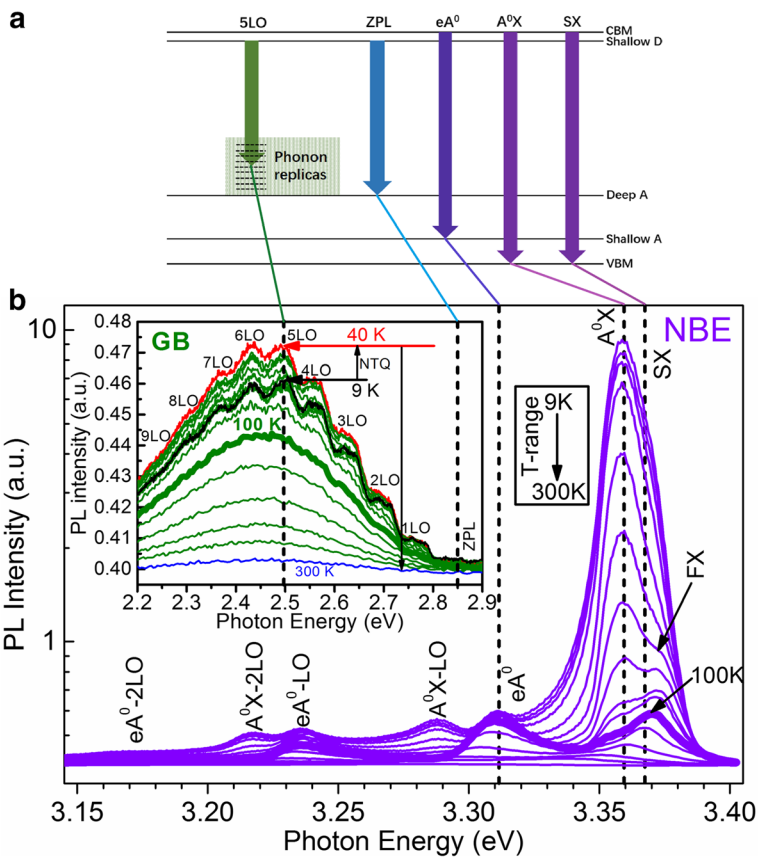

Fig. 4 The TD-PL spectra of the N-doped ZnO MRs recorded from 9 to 300 K at the NBE region. The *inset* shows the corresponding GB emissions. The *top panel* draws a schematic energy band diagram and marks the origin of the GB, eA^0, and A^0X emissions, respectively

N-doped ZnO MRs is assigned to excitons bound to neutral acceptors (A^0X) [27–29]. Considering the free exciton (FX) line at 3.377 eV, the acceptor here is a shallow acceptor with its binding energy of around 18 meV. Due to the uncertainty of the Haynes factor for acceptors in ZnO, it is difficult to give the accurate energy level of this shallow acceptor. Taking the Haynes factor of 0.1–0.2, the energy level is around 90–180 meV [30]. Regarding the identification of the shallow acceptor in N-doped ZnO materials, there is no unified conclusion until now. The N_O was widely considered as a shallow acceptor for a long time. However, recent calculations demonstrated that the N_O has an exceedingly high ionization energy of 1.3 eV [31], supported by the experimental results of Huang et al. [32], which means N_O is not the natural candidate for explaining the observed A^0X. Lately, more and more papers have a tendency to assign the unidentified shallow acceptor to a *native-extrinsic* complex or native defect *cluster* complex, including $2V_{Zn} - D_{Zn}$ (D = P, As, Sb) [33, 34], $V_{Zn} - N_O$ [13], $2V_{Zn} - V_O$ [35], $3V_{Zn} - D_i$ (D = P, As, Sb) [36], and V_{Zn} clusters [16]. In fact, the successful demonstration of ZnO homo-junction-based light-emitting devices [37] and even laser diodes [38] undoubtedly supports the existence of shallow acceptor state(s) in group VA-doped ZnO materials. In our case, considering the chemicals incorporated, it is highly possible that the shallow acceptors in N-doped ZnO MRs be $V_{Zn} - N_O$ or V_{Zn} clusters since N signals are detectable by XPS and energy-dispersive spectra [12].

In addition to the A^0X and FX, a shoulder at 3.368 eV must be added for a better fitting of the NBE region. Regarding the assignment, it has been reported that surface exciton (SX) emission may occur in this spectral range, especially for ZnO nanostructures because of the large surface-volume ratio [39]. Moreover, the temperature dependence of the peak shows that the intensity decreases dramatically with increasing temperature, which is a typical behavior of SX [12]. Therefore, we attribute the shoulder at 3.368 eV to SX, which originates from the ionized bound excitons due to the surface depletion. For the attribution of the hump at 3.311 eV, according to our previous study and the temperature dependence of the peak position [12], we ascribe it to free electrons to acceptors (eA^0). The acceptor state is thus around 120–130 meV, which is consistent with the acceptors responsible for A^0X. The rest peaks at the lower energy side are ascribed to the first and second LO phonon replica of A^0X or eA^0, which have been denoted in Fig. 3 correspondingly. In addition, the GB emissions with zero-phonon line (ZPL) around 2.85 eV and its nine LO phonon replicas are presented in the inset of Fig. 4. It is found that the intensity of the GB increases first with increasing measuring temperature until 40 K, and this anomalous phenomenon is called negative thermal quenching effect which further ensures that the GB emissions in N-doped ZnO MRs originate from shallow donors to the isolated V_{Zn} with a relatively deep acceptor energy level [11, 12]. Note that the GB intensity (~0.47) is negligible as compared to that of the NBE (~10); it thus implies that shallow donors are suppressed to some extent, which is consistent with Raman spectrum.

In order to obtain the electrical properties of the N-doped ZnO MRs, field-effect transistors (FETs) of individual MRs were fabricated by standard photolithography. N-doped ZnO MRs were first transferred to a p^+-silicon wafer with a 200-nm thick silicon oxide on the surface, which served as the back-gate electrode of the transistor. Microcontact windows were defined on the ends of the MRs, and then, the electrodes with 10 nm of Ni followed by 150 nm of Au were formed by electron-beam evaporator and subsequent lift-off. The inset in Fig. 5 shows the SEM image of the N-doped ZnO MR FET, and the channel length between the electrodes is around 3 μm. Meanwhile, the drain current (I_d) versus gate voltage (V_g) curve under a drain voltage (V_d) of 10 V is shown in Fig. 5. According to the literature [40], the carrier concentration (Q) in N-doped ZnO MR can be estimated by the following equation: $Q = (V_{th}/e)[2\pi\varepsilon_r\varepsilon_0/\ln(4h/d)]/(\pi d^2/4)$, where V_{th}, e, ε_r, ε_0, h, and d are the threshold voltage obtained from the transconductance in Fig. 5, the electron charge, the effective dielectric constant (3.9 for SiO_2), the dielectric constant in vacuum, the thickness of gate oxide layer, and MR diameter (~1 μm), respectively. The carrier concentration is thus estimated to be $\sim 2.3 \times 10^{15}$ cm^{-3}. The high resistance of the MR implies the existence of acceptors, which is consistent with the PL signatures of shallow and deep acceptors related to V_{Zn}.

Utilizing the optical signatures of the native defects, one can easily establish the relation between native defects

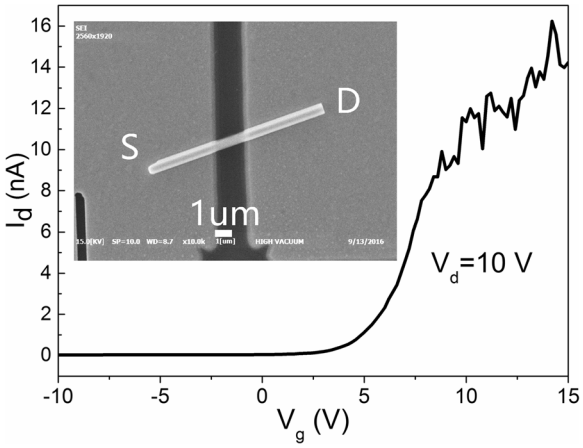

Fig. 5 The I_d–V_g curve of the N-doped ZnO MR FET under V_d = 10 V. The *inset* shows the SEM image of the FET

and the radiative emission. However, the spatial resolution for usual PL system is well above the micrometer range, which leads to averaging over many N-doped ZnO MRs on the sample surface. Although PL measurement on individual submicron structures is possible, the accuracy of the technique is limited by the diffraction limit and poor signal-to-noise ratio [6]. In order to gain insight on the local luminescence properties of a single N-doped ZnO MR and to reveal the distribution of native point defect, an approach is to measure the optical response via a luminescence spectroscopy with a scanning tunneling microscope (STM), which is acquired by retracting the STM tip from the sample surface for a few 100 nm [41, 42]. Another economic approach is to use the SR-CL spectra equipped within a regular SEM system [4–10], which is also of high spatial resolution due to the very tiny spot size of the electron beam. As a result, the SR-CL and monochromatic imaging were performed in a sample area of $6 \times 4.8\ \mu m^2$ with an acceleration voltage of 15 kV at 100 K.

Figure 6a shows the top view SEM image of one single hexagonally shaped N-doped ZnO MR in the investigated area, while the CL monochromatic 2D mapping of this MR recorded at a photon energy of 3.306 eV (375 nm) and 2.480 eV (500 nm) are shown in Fig. 6b, c, respectively. It can be noticed that the ultraviolet luminescence is stronger at the center of the MR, but in contrast, the green band luminescence mainly originates from the edge within a thickness of around 200–300 nm. Taking the

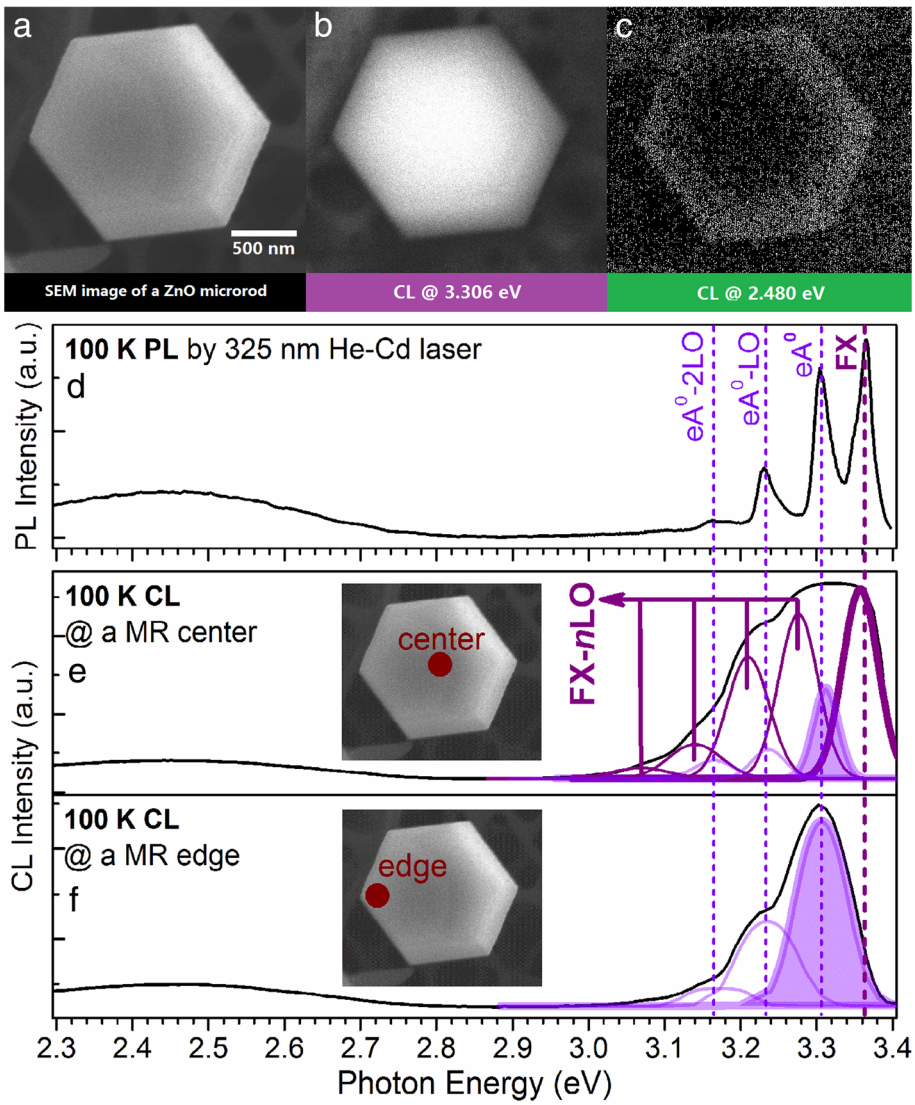

Fig. 6 The SR-CL spectra and monochromatic images of a single N-doped ZnO MR performed with an accelerating voltage of 15 kV at 100 K. **a** The top view SEM image of the selected MR. **b** The CL monochromatic mapping of the MR taken at 3.306 eV. **c** The CL monochromatic mapping of the MR taken at 2.480 eV. **d** The PL spectrum measured at 100 K. **e** The CL spectrum obtained in spot mode from the center of the MR. **f** The CL spectrum obtained in spot mode from the edge of the MR

advantage of high spatial resolution of the CL technique, Fig. 6e, f presents two CL spectra obtained in spot mode from the center and edge, respectively. Figure 6d shows the 100 K PL spectrum for identification of the optical transitions in the CL spectra. By comparing the CL spectra with the PL spectrum, the 3.306 eV peak corresponds to the eA^0 while the 2.480 eV peak corresponds to the GB. Owing to the width of CL spectra that are much larger than that of the PL, peak deconvolution process has been employed for the CL spectra according to the well-resolved PL peaks. As can be seen from the deconvoluted components, the intensified eA^0 emission at the center observed in Fig. 6b actually originates from the contribution of FX and its first LO-phonon replica whereas the actual intensity of eA^0 emission at the center is weaker than that at the edge. As the eA^0 is linked to the shallow acceptors, the result indicates that more shallow acceptors are located along the edge of the MR. For the GB luminescence, the integrated intensity ratio of the GB/NBE is 0.179 and 0.342 for center and edge, respectively, indicating that more isolated V_{Zn} defects are located near the edge area, similar to the monochromatic observation from Fig. 6c.

In fact, the inhomogeneous distribution of the acceptor-like defects occurs not only between the center and edge of the MRs but also between the top surface and the bulk underneath the surface. To attest this issue, depth-resolved CL measurement at 100 K has been carried out with various acceleration voltages at the center point. Figure 7 shows the CL spectra recorded at five different acceleration voltages of 3, 6, 9, 12, and 15 kV, which correspond to the respective average generation depths of 40, 110, 210, 340, and 500 nm in ZnO material, according to the calculation results through the Monte-Carlo simulation CASINO in literature [43]. As plotted in the inset of Fig. 7, the integrated intensity ratio of eA^0/FX and GB/FX both decreases with increasing acceleration voltage due to the core of the N-doped ZnO MR has relatively less V_{Zn}-related acceptor-like complexes.

The inhomogeneous distribution of the acceptor-like defects can be unified to the difference between surface and bulk. It is a well-known fact that surface defects of metal oxides function as adsorption sites [44]. The adsorption of a gas molecule, such as O_2 or H_2O, on the surface of ZnO will trap the free electrons to form negative O_2^- or OH^- ions. Therefore, the adsorbates acting as acceptors deplete the surface electron states, leaving behind positively charged native defects or dopants near the surface, resulting in the space charge region and band bending of the surface [45, 46]. Due to larger surface-to-volume ratio, such a surface effect is more significant on ZnO nanostructures, compared with bulk materials. A layer that is depleted of mobile electrons is then created at the surface of the ZnO MR, the width of which is up to more than 100 nm [47]. Moreover, it has been reported that the V_{Zn}^- centers only exist in the depletion layer [48], which could compensate for an intrinsic charge imbalance. In addition to the results reported by Fabbri et al. [10], all the above discussions suggest that both the V_{Zn}-related complex shallow acceptors and the isolated V_{Zn} deep acceptors are mainly located near the surface region of the MRs. The intensified FX in bulk area and the disappearance of the peak at the surface area indicate that the crystalline quality is relatively better in bulk and relatively worse at surface. Possibly, for this very reason, more acceptor-like isolated and complex defects can form at the MR surface region. The "core-shell" luminescent structure of the N-doped ZnO MRs has been schematically drawn in Fig. 8. With further

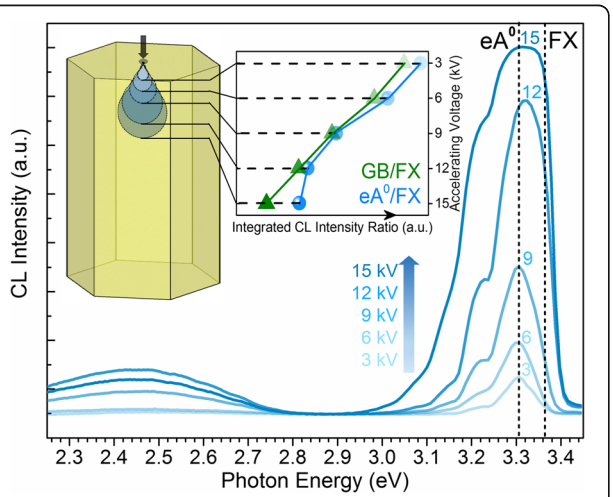

Fig. 7 The CL spectra taken at 100 K in spot mode at the center of the N-doped ZnO MR with five different acceleration voltages of 3, 6, 9, 12, and 15 kV. The *inset* shows the integrated intensity ratio of eA^0/FX and GB/FX as a function of the accelerating voltage (i.e., detection depth)

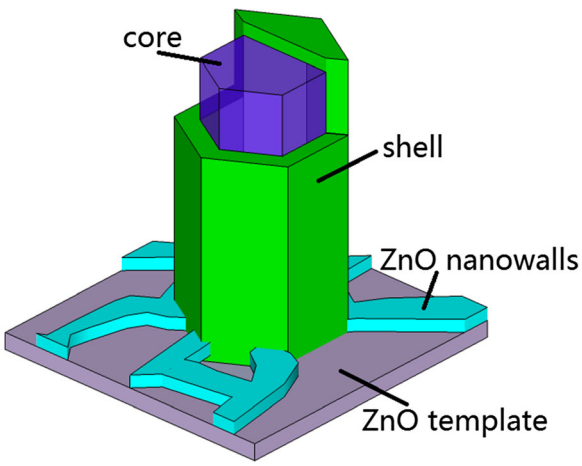

Fig. 8 The schematic model of one N-doped ZnO MR with core-shell-structured luminescent inhomogeneity

design and optimization of the experiment conditions, it might be possible to achieve a co-axial p–n junction which can be potentially applied to co-axial light-emitting devices.

Conclusions

In conclusion, vertically aligned N-doped ZnO MRs with excellent crystalline quality were carried out via the chemical vapor transport method. The experimental results of Raman and TD-PL investigations demonstrate that the shallow donor-like defect Zn_i has been suppressed in O-rich growth environment, while on the other hand, N incorporation induced shallow acceptor state: V_{Zn}-related complex or clusters are stable. Through comprehensive comparison between SR-CL spectra and monochromatic images taken at 100 K, we find the luminescent inhomogeneity of N-doped ZnO MRs, which has core-shell structure. The isolated V_{Zn} connected with the GB- and V_{Zn}-related complexes or clusters associated with the eA^0 emission mainly distributes in the shell of a thickness about 200–300 nm. The present study has provided a microscopic model for the distribution of acceptors in N-doped ZnO micro-/nanostructures and is certainly crucial for further design of one-dimensional ZnO nanostructure devices.

Abbreviations

A^0X: Excitons bound to neutral acceptor; CL: Cathodoluminescence; D^0X: Excitons bound to neutral donor; DL: Deep-level; FET: Field-effect transitor; FWHM: Full width at half maximum; FX: Free exciton; GB: Green band; LO: Longitudinal optical; MR: Microrod; NBE: Near band edge; PL: Photoluminescence; SEM: Scanning electron microscope; SR: Spatially resolved; STM: Scanning tunneling microscope; SX: Surface exciton; TD: Temperature-dependent; VLS: Vapor–liquid–solid; V_O: Oxygen vacancy; V_{Zn}: Zinc vacancy; XPS: X-ray photoelectron spectrometry; XRD: X-ray diffraction; ZPL: zero-phonon line

Acknowledgements

This research was supported by the State Key Program for Basic Research of China under Grant No. 2011CB302003, National Natural Science Foundation of China (Nos. 61274058, 61322403, 61504057, and 61574075), the Natural Science Foundation of Jiangsu Province (Nos. BK20130013 and BK20150585), and the Six Talent Peaks Project in Jiangsu Province (2014XXRJ001). Special thanks to Prof. Hai Lu and Mr. Wenkai Liu for their help of the nano-fabrication and electrical test.

Funding

This study was funded by the State Key Program for Basic Research of China (2011CB302003), the National Natural Science Foundation of China (61274058, 61322403, 61504057, and 61574075), the Natural Science Foundation of Jiangsu Province (BK20130013 and BK20150585), and the Six Talent Peaks Project in Jiangsu Province (2014XXRJ001).

Authors' Contributions

ZRY did the material growth and some measurement (XPS, XRD, Raman, TD-PL, and SR-CL) and wrote the paper. KT proposed the initial work and finalized the manuscript. ZHX did some measurement (SEM and SR-CL). SMZ and JDY participated in some of the design and experimental work of this study. SLG supervised the work. All authors read and approved the final manuscript.

Competing Interests

The authors declare that they have no competing interests.

Author details

[1]School of Electronic Science and Engineering, Nanjing University, Nanjing 210023, China. [2]School of Science, China Pharmaceutical University, Nanjing 211198, China.

Received: 21 April 2016 Accepted: 16 November 2016
Published online: 22 November 2016

References

1. Janotti A, Van de Walle CG (2009) Fundamentals of zinc oxide as a semiconductor. Rep Prog Phys 72:126501
2. Reynolds JG, Reynolds CL (2014) Progress in ZnO acceptor doping: what is the best strategy. Adv Condens Matter Phys 2014:457058
3. Heinze S, Dadgar A, Bertram F et al (2007) Metalorganic vapor phase epitaxy of ZnO: toward p-type conductivity. Proc SPIE 6474:647406
4. Shalish I, Temkin H, Narayanamurti V (2004) Size-dependent surface luminescence in ZnO nanowires. Phys Rev B 69:245401
5. Pan N, Wang XP, Li M et al (2007) Strong surface effect on cathodoluminescence of an individual tapered ZnO nanorod. J Phys Chem C 111:17265–17267
6. Foley M, Ton-That C, Phillips MR (2008) Cathodoluminescence inhomogeneity in ZnO nanorods. Appl Phys Lett 93:243104
7. Khranovskyy V, Lazorenko V, Lashkarev G et al (2012) Luminescence anisotropy of ZnO microrods. J Lumin 132:2643–2647
8. Liao X, Zhang X (2007) Zinc oxide nanostructures and their core-shell luminescence properties. J Phys Chem C 111:9081–9085
9. Kaftelen H, Ocakoglu K, Thomann R et al (2012) EPR and photoluminescence spectroscopy studies on the defect structure of ZnO nanocrystals. Phys Rev B 86:014113
10. Fabbri F, Villani M, Catellani A et al (2014) Zn vacancy induced green luminescence on non-polar surfaces in ZnO nanostructures. Sci Rep 4:5158
11. Chen H, Gu SL, Tang K et al (2011) Origins of green band emission in high-temperature annealed N-doped ZnO. J Lumin 131:1189–1192
12. Yao ZR, Gu SL, Tang K et al (2015) Zinc vacancy related emission in homoepitaxial N-doped ZnO microrods. J Lumin 161:293–299
13. Liu L, Xu J, Wang D et al (2012) p-Type conductivity in n-doped ZnO: the role of the N_{Zn}–V_O complex. Phys Rev Lett 108:215501
14. Reynolds JG, Reynolds CL Jr, Mohanta A et al (2013) Shallow acceptor complexes in p-type ZnO. Appl Phys Lett 102:152114
15. Børseth TM, Tuomisto F, Christensen JS et al (2008) Vacancy clustering and acceptor activation in nitrogen-implanted ZnO. Phys Rev B 77:045204
16. Tuomisto F, Rauch C, Wagner MR et al (2013) Nitrogen and vacancy clusters in ZnO. J Mater Res 28:1977–1983
17. Ng HT, Li J, Smith MK et al (2003) Growth of epitaxial nanowires at the junctions of nanowalls. Science 300:1249
18. Grabowska J, Meaney A, Na KK et al (2005) Surface excitonic emission and quenching effects in ZnO nanowire/nanowall systems: limiting effects on device potential. Phys Rev B 71:115439
19. Hu JQ, Li Q, Wong NB et al (2002) Synthesis of uniform hexagonal prismatic ZnO whiskers. Chem Mater 14:1216–1219
20. Perkins CL, Lee SH, Li X et al (2005) Identification of nitrogen chemical states in N-doped ZnO via x-ray photoelectron spectroscopy. J Appl Phys 97:034907
21. Wei H, Wu Y, Wu L et al (2005) Preparation and photoluminescence of surface N-doped ZnO nanocrystal. Mater Lett 59:271–275
22. Major S, Kumar S, Bhatnagar M et al (1986) Effect of hydrogen plasma treatment on transparent conducting oxides. Appl Phys Lett 49:394–396
23. Chen M, Wang X, Yu YH et al (2000) X-ray photoelectron spectroscopy and auger electron spectroscopy studies of Al-doped ZnO films. Appl Surf Sci 158:134–140
24. Janotti A, Van de Walle CG (2007) Native point defects in ZnO. Phys Rev B 76:165202
25. Gluba MA, Nickel NH, Karpensky N (2013) Interstitial zinc clusters in zinc oxide. Phys Rev B 88:245201
26. Zhang P, Kong CY, Li WJ et al (2015) The origin of the ~274 cm^{-1} additional Raman mode induced by the incorporation of N dopants and a feasible route to achieve p-type ZnO: N thin films. Appl Surf Sci 327:154–158
27. Meyer BK, Alves H, Hofmann DM et al (2004) Bound exciton and donor–acceptor pair recombinations in ZnO. Phys Stat Sol B 241:231–260
28. Xiu FX, Yang Z, Mandalapu LJ et al (2005) High-mobility Sb-doped p-type ZnO by molecular-beam epitaxy. Appl Phys Lett 87:152101

29. Huang J, Chu S, Kong JY et al (2013) ZnO p-n homojunction random laser diode based on nitrogen-doped p-type nanowires. Adv Optical Mater 1:179–185
30. Tang K, Gu SL, Ye JD et al (2012) Temperature-dependent photoluminescence of ZnO films codoped with tellurium and nitrogen. J Appl Phys 112:103534
31. Lyons JL, Janotti A, Van de Walle CG (2009) Why nitrogen cannot lead to p-type conductivity in ZnO. Appl Phys Lett 95:252105
32. Huang R, Xu S, Guo W et al (2011) Nitrogen deep accepters in ZnO nanowires induced by ammonia plasma. Appl Phys Lett 99:143112
33. Limpijumnong S, Zhang SB, Wei SH et al (2004) Doping by large-size-mismatched impurities: the microscopic origin of arsenic- or antimony-doped p-type zinc oxide. Phys Rev Lett 92:155504
34. Lee WJ, Kang J, Chang KJ (2006) Defect properties and p-type doping efficiency in phosphorus-doped ZnO. Phys Rev B 73:024117
35. Bang J, Kim YS, Park CH et al (2014) Understanding the presence of vacancy clusters in ZnO from a kinetic perspective. Appl Phys Lett 104:252101
36. Puchala B, Morgan D (2012) Stable interstitial dopant-vacancy complexes in ZnO. Phys Rev B 85:195207
37. Nakahara K, Akasaka S, Yuji H et al (2010) Nitrogen doped $Mg_xZn_{1-x}O$/ZnO single heterostructure ultraviolet light-emitting diodes on ZnO substrates. Appl Phys Lett 97:013501
38. Chu S, Wang GP, Zhou WH et al (2011) Electrically pumped waveguide lasing from ZnO nanowires. Nat Nanotechnol 6:506–510
39. Richters JP, Voss T, Wischmeier L et al (2008) Influence of polymer coating on the low-temperature photoluminescence properties of ZnO nanowires. Appl Phys Lett 92:011103
40. Martel R, Schmidt T, Shea HR et al (1998) Single-and multi-wall carbon nanotube field-effect transistors. Appl Phys Lett 73:2447–2449
41. Stavale F, Nilius N, Freund HJ (2013) STM luminescence spectroscopy of intrinsic defects in ZnO (0001) thin films. J Phys Chem Lett 4:3972–3976
42. Stavale F, Pascua L, Nilius N et al (2014) Luminescence properties of nitrogen-doped ZnO. J Phys Chem C 118:13693–13696
43. Ton-That C, Phillips MR (2015) Cathodoluminescence microanalysis of ZnO nanowires. In: Arbiol J, Xiong Q, editors. Semiconductor Nanowires: Materials, Synthesis, Characterization and Application. Elsevier, p. 398
44. Henrich VE, Cox PA (1994) Surface science of metal oxides. Cambridge University Press, p. 288
45. Liao ZM, Zhang HZ, Zhou YB et al (2008) Surface effects on photoluminescence of single ZnO nanowires. Phys Lett A 372:4505–4509
46. Hu Y, Liu Y, Li W et al (2009) Observation of a 2D electron gas and the tuning of the electrical conductance of ZnO nanowires by controllable surface band-bending. Adv Funct Mater 19:2380–2387
47. Liu ZW, Ong CK, Yu T et al (2006) Catalyst-free pulsed-laser-deposited ZnO nanorods and their room-temperature photoluminescence properties. Appl Phys Lett 88:053110
48. Wu XL, Siu GG, Fu CL et al (2001) Photoluminescence and cathodoluminescence studies of stoichiometric and oxygen-deficient ZnO films. Appl Phys Lett 78:2285–2287